10264 *Inorg. Chem.* **2010**, *49*, 10264–10272
DOI: 10.1021/ic9018794

Inorganic Chemistry
Article

Quinonoid-Bridged Chair-Shaped Dirhenium(I) Metallacycles: Synthesis, Characterization, and Spectroelectrochemical Studies

Dibyendu Bhattacharya,[†] Malaichamy Sathiyendiran,[†] Jing-Yun Wu,[‡] Che-Hao Chang,[†] Sung-Chou Huang,[‡] Yu-Ling Zeng,[‡] Ching-Yao Lin,[‡] P. Thanasekaran,[†] Bo-Chao Lin,[†] Chao-Ping Hsu,[†] Gene-Hsiang Lee,[§] Shie-Ming Peng,[§] and Kuang-Lieh Lu*[,†]

[†]*Institute of Chemistry, Academia Sinica, Taipei 115, Taiwan,* [‡]*Department of Applied Chemistry, National Chi Nan University, Nantou 545, Taiwan, and* [§]*Department of Chemistry, National Taiwan University, Taipei 107, Taiwan*

Received September 22, 2009

Self-assembled, chair-shaped dirhenium(I) macrocyclic compounds featuring the two different bis-chelating quinone dianions (**1**, L = $dhnq^{2-}$; **2**, L = $dhaq^{2-}$; H_2dhnq = 6,11-dihydroxy-5,12-naphthacenedione; H_2dhaq = 1,4-dihydroxy-9,10-anthraquinone) that interface with two *fac*-$Re(CO)_3$ cores and a ditopic semirigid *N*-donor 1,4-bis(5,6-dimethylbenzimidazol-1-ylmethyl)naphthalene (L′ = *p*-NBimM) ligand coordinated to the remaining orthogonal site were prepared in high yields. Their structures were confirmed by single-crystal X-ray diffraction analysis. Electrochemical assessments, using cyclic voltammetry (CV) and UV−vis−NIR spectroelectrochemistry (SEC), revealed the existence of two well-separated, single-electron quinone ligand-centered, reversibly accessible 0, −1, and −2 redox states. Among the two singly reduced radical complexes, the symmetrically bridged quinone complex $\mathbf{1}^{\bullet-}$, showed a strong absorption in the NIR regions, which was not observed for the neutral and doubly reduced states, analogous to that of the free $dhnq^{3\bullet-}$ quinone. In contrast, when **2** was reduced to $\mathbf{2}^{\bullet-}$, a broad signal at 866 nm was observed, very similar to the reduced $dhaq^{3\bullet-}$ quinone. This difference in spectral behavior in the singly reduced states is likely due to the annealed benzene ring in **1** and $dhnq^{2-}$ because of its symmetrical π-electron system, which is perturbed to a lesser degree compared to asymmetric **2** and $dhaq^{2-}$. Reduction to $\mathbf{1}^{\bullet-}$ produces a small but not negligible *g* factor anisotropy ($\Delta g = 0.024$) in the electron spin resonance (ESR) signal, indicative of a very small metal-centered spin (5%), but $\mathbf{2}^{\bullet-}$ shows a *g* value in the expected range for organic radicals (no detectable Δg). Thus, the combined investigations reveal that the singly reduced metallacycles are best described as being highly stable, noncommunicating, localized, quinonoid-centered radical complexes, $[(CO)_3Re^{I}(\mu\text{-}L^{3\bullet-})(\mu\text{-}L')Re^{I}(CO)_3]^{\bullet-}$.

Introduction

Ligand-bridged dimetallic systems, along with selective redox-active quinonoid ligands, have attracted considerable interest in recent years due to the fact that the intramolecular electronic coupling processes can be tuned in their mixed-valence (MV) states,[1] which, in turn, provides an opportunity for understanding the energy and electron-transfer processes[2] and their biological importance in systems ranging from quinoproteins to photosystems.[3] Depending on the relative energies of the redox-active orbitals, dimetallic complexes with proradical ligands can be characterized as metal−ligand radicals, $[M^n(\mu\text{-}L)(\mu\text{-}L')M^{n+1}]$ (type A) or $[M^{n+0.5}(\mu\text{-}L)(\mu\text{-}L')\text{-}M^{n+0.5}]$ (type B) or as a radical complex $[M^n(\mu\text{-}L^{\bullet-})(\mu\text{-}L')M^n]$ (type C).[1b,4] Particularly interesting from a fundamental perspective are the interactions of the unpaired electron of the ligand with either the metal or another ligand (superexchange interactions through covalent bonds or through space electronic communication), which affects the behavior of electronic

*To whom correspondence should be addressed. Fax: 886(2)27831237. E-mail: lu@chem.sinica.edu.tw.

(1) (a) Das, A. K.; Sarkar, B.; Fiedler, J.; Zális, S.; Hartenbach, I.; Strobel, S.; Lahiri, G. K.; Kaim, W. *J. Am. Chem. Soc.* **2009**, *131*, 8895. (b) Kumbhakar, D.; Sarkar, B.; Maji, S.; Mobin, S. M.; Fiedler, J.; Urbanos, F. A.; Jiménez-Aparicio, R.; Kaim, W.; Lahiri, G. K. *J. Am. Chem. Soc.* **2008**, *130*, 17575. (c) Prassides, K. In *Mixed Valency Systems - Applications in Chemistry, Physics and Biology*; Kluwer Academic Publishers: Dordrecht, The Netherlands, 1991. (d) Fabre, M.; Bonvoisin, J. *J. Am. Chem. Soc.* **2007**, *129*, 1434. (e) Manriquez, J. M.; Yee, G. T.; McLean, R. S.; Epstein, A. J.; Miller, J. S. *Science* **1991**, *252*, 1415. (f) Maji, S.; Sarkar, B.; Mobin, S. M.; Fiedler, J.; Urbanos, F. A.; Aparicio, R. J.; Kaim, W.; Lahiri, G. K. *Inorg. Chem.* **2008**, *47*, 5204. (g) Ward, M. D.; McCleverty, J. A. *J. Chem. Soc., Dalton Trans.* **2002**, 275. (h) Pierpont, C. G. *Coord. Chem. Rev.* **2001**, *216*, 99.

(2) (a) Heyduk, A. F.; Nocera, D. G. *Science* **2001**, *293*, 1639. (b) Esswein, A. J.; Veige, A. S.; Piccoli, P. M. B.; Schultz, A. J.; Nocera, D. G. *Organometallics* **2008**, *27*, 1073. (c) Reece, S. Y.; Seyedsayamdost, M. R.; Stubbe, J.; Nocera, D. G. *J. Am. Chem. Soc.* **2006**, *128*, 13654. (d) Rendina, L. M.; Puddephatt, R. *J. Chem. Rev.* **1997**, *97*, 1735. (e) Periana, R. A.; Taube, D. J.; Gamble, S.; Taube, H.; Satoh, T.; Fujii, H. *Science* **1998**, *280*, 560. (f) Shavaleev, N. M.; Accorsi, G.; Virgili, D.; Bell, Z. R.; Lazarides, T.; Calogero, G.; Armaroli, N.; Ward, M. D. *Inorg. Chem.* **2005**, *44*, 61. (g) Van Wallendael, S.; Shaver, R. J.; Rillema, D. P.; Yoblinski, B. J.; Stathis, M.; Guarr, T. F. *Inorg. Chem.* **1990**, *29*, 1761.

 Published on Web 10/14/2010

coupling in the mixed-valence state.[5,6] It is noteworthy that few examples of coordination compounds feature ligands rather than metal ions as electron donors and acceptors. Tetra- or hexa-Re(I) complexes with either bipyridyl or triazine ligand-centered MV systems are prime candidates for realizing direct through space electronic communication.[5] Electron transfer via superexchange may be the dominant mechanism, provided the energy of the lowest unoccupied molecular orbital of the bridging ligand is close to that of the donor and acceptor moieties, since the comparable energies of the bridge and metal redox centers would act to reduce the activation barrier to electron tunneling.[6,7] Therefore, dinuclear ruthenium(II) complexes bridged by *o*- and *p*-quinonoid molecules in combination with different coligands and mixed-valence systems have been scrutinized in detail.[1a,b,7] However, the subtleties of quinonoid−rhenium(I) behavior, which underlie the importance of these compounds, have yet to be explored.

Herein, we report on the synthesis (in a one step assembly) of the chair-shaped, neutral dirhenium(I) metallacycles, $[(CO)_3Re^I(\mu\text{-L})(\mu\text{-L}')Re^I(CO)_3]$, (**1**, L = $dhnq^{2-}$; **2**, L = $dhaq^{2-}$; H_2dhnq = 6,11-dihydroxy-5,12-naphthacenedione; H_2dhaq = 1,4-dihydroxy-9,10-anthraquinone) and a ditopic semirigid *N*-donor ligand, 1,4-bis(5,6-dimethylbenzimidazol-1-ylmethyl)-naphthalene (L′ = *p*-NBimM). The ligand valence state distribution in $\mathbf{1}^n$ and $\mathbf{2}^n$, where $n = 0$, -1, and -2, was assessed via CV and UV−vis−NIR SEC. Type C quinone-containing radical complexes, $[(CO)_3Re^I(\mu\text{-L}^{3\bullet-})(\mu\text{-L}')Re^I(CO)_3]^{\bullet-}$, produced via the reduction of neutral dirhenium(I) metallacycles show the following features: (1) quinone ligand-centered; two well-separated, single-electron, reversibly accessible 0, −1, −2 redox states. The benziimidazolate ligand appears to be redox innocent within the solvent window: (2) small-to-negligible *g*-factor anisotropy in the ESR signal, signifying $a \leq 5\%$ metal-centered spin in the singly reduced states, and (3) highly stable, noncommunicating, localized, quinonoid-centered radical complexes, as evidenced by combined SEC and ESR data. The electronic characteristics of the radical-anionic and dianionic states of such biologically relevant quinonoid ligands in the forms of free and Re(I) complexes are described for the first time.

Experimental Section

Materials. All starting materials and products were stable toward moisture and air. Commercial grade reagents, $Re_2(CO)_{10}$, 6,11-dihydroxy-5,12-naphthacenedione (H_2-dhnq), and 1,4-dihydroxy-9,10-anthraquinone (H_2-dhaq), were used as received. The solvents used in this study were of spectroscopic grade.

Physical Measurements and Procedures. Elemental analyses for carbon, hydrogen, and nitrogen were recorded with a Perkin-Elmer 2400 CHN elemental analyzer. Infrared spectra were measured on a Perkin-Elmer PARAGON 1000 FT-IR spectrometer. ^{1}H NMR spectra were recorded on Bruker AC 300 and AMX-400 FT-NMR spectrometers. FAB-MS data were obtained using a JEOL JMS-700 double focusing mass spectrometer. The electronic absorption spectra were obtained on a Hewlett-Packard 8453 spectrophotometer at room temperature in a 1 cm quartz cell. Fluorescence spectra were recorded on a Hitachi F4500 spectrometer. Excited-state lifetimes were measured as described previously.[5d] Cyclic voltammograms (CV) and differential pulse voltammograms (DPV) were measured in anhydrous DMSO/0.1 M Bu_4NClO_4 as a supporting electrolyte at 298 K. CVs were carried out at a 100 mV/s scan rate, using a three-electrode configuration (Pt working electrodes, Pt wire counter electrode, and saturated calomel electrode (SCE) reference electrode) and a CHI Electrochemical Workstation 611A under deaerated conditions. UV−vis−NIR spectroelectrochemistry was performed with an airtight, optically transparent thin-layer electrochemical cell (OTTLE) constructed with a 100 mesh platinum gauze working electrode in a 1 mm quartz cell.[8] UV−vis−NIR spectra were recorded with a JASCO V-570 UV−vis−NIR spectrophotometer. Both electrolysis cells were assembled under an inert atmosphere in a glovebox equipped with a drytrain to exclude moisture and oxygen.

Crystallographic Determination. Suitable single crystals of $\mathbf{1}\cdot C_7H_8$ and $\mathbf{2}\cdot C_7H_8$ with dimensions of 0.30 × 0.30 × 0.15 mm and 0.25 × 0.20 × 0.15 mm, respectively, were selected for indexing and the collection of intensity data. Measurements were performed using graphite-monochromatized Mo Kα radiation (λ = 0.71073 Å) on a Nonius Kappa CCD diffractometer. Intensity data were collected at 150(2) K within the limits $1.59° < \theta < 27.49°$ for $\mathbf{1}\cdot C_7H_8$ and $1.38° < \theta < 27.50°$ for $\mathbf{2}\cdot C_7H_8$. The structures were solved by direct methods and refined on F^2 by full-matrix least-squares calculations using SHELX-97 program packages.[9] Because of the disordered syndrome of guest molecules, the carbon atoms of the toluene molecules in $\mathbf{2}\cdot C_7H_8$ were refined isotropically. Other non-hydrogen atoms were refined anisotropically, and all hydrogen atoms were assigned by geometrical calculation and refined as riding models. Details of the structure determinations are given

(3) (a) Robert, R.; David, S.; Annemarie, S.; Eskouhie, T.; Andrea, F. *Nature* **2005**, *433*, 7025. (b) Hiroshi, S.; Knapp, E.-W. *J. Am. Chem. Soc.* **2005**, *127*, 14714. (c) Fufezan, C.; Gross, C. M.; Sjodin, M.; Rutherford, A. W.; Krieger-Liszkay, A.; Kirilovsky, D. *J. Biol. Chem.* **2007**, *282*, 12492. (d) Davidson, V. L. In *Principles and Applications of Quinoproteins*; Marcel Dekker: New York, 1993. (e) Klinman, J. P.; Mu, D. *Annu. Rev. Biochem.* **1994**, *63*, 299. (f) Dooley, D. M. *J. Biol. Inorg. Chem.* **1999**, *4*, 1. (g) Duine, J. A. *Eur. J. Biochem.* **1991**, *200*, 271. (h) Duine, J. A. *J. Biosci. Bioeng.* **1999**, *88*, 231. (i) Goodwin, P. M.; Anthony, C. *Adv. Microb. Physiol.* **1998**, *40*, 1. (j) Duine, J. A.; Jongejan, J. A. In *Bioinorganic Catalysis*; Reedijk, J., Ed.; Marcel Dekker: New York, 1993; p 447. (k) Klinman, J. P. *Proc. Natl. Acad. Sci. U.S.A.* **2001**, *98*, 705. (l) Mure, M.; Mills, S. A.; Klinman, J. P. *Biochemistry* **2002**, *41*, 9269. (m) Bollinger, J. A.; Brown, D. E.; Dooley, D. M. *Biochemistry* **2005**, *44*, 11708. (n) Mure, M.; Wang, S. X.; Klinman, J. P. *J. Am. Chem. Soc.* **2003**, *125*, 6113.

(4) (a) Shimazaki, Y.; Stack, T. D. P.; Storr, T. *Inorg. Chem.* **2009**, *48*, 8383. (b) Kaim, W.; Lahiri, G. K. *Angew. Chem., Int. Ed.* **2007**, *46*, 1778.

(5) (a) Dinolfo, P. H.; Coropceanu, V.; Brédas, J.-L.; Hupp, J. T. *J. Am. Chem. Soc.* **2006**, *128*, 12592. (b) Dinolfo, P. H.; Williams, M. E.; Stern, C. L.; Hupp, J. T. *J. Am. Chem. Soc.* **2004**, *126*, 12989. (c) Dinolfo, P. H.; Lee, S. J.; Coropceanu, V.; Brédas, J. L.; Hupp, J. T. *Inorg. Chem.* **2005**, *44*, 5789. (d) Bhattacharya, D.; Sathiyendiran, M.; Luo, T.-T.; Chang, C.-H.; Cheng, Y.-H.; Lin, C.-Y.; Lee, G. H.; Peng, S.-M.; Lu, K.-L. *Inorg. Chem.* **2009**, *48*, 3731. (e) Kaim, W.; Schwederski, B.; Dogan, A.; Fiedler, J.; Kuehl, C. J.; Stang, P. J. *Inorg. Chem.* **2002**, *41*, 4025.

(6) (a) Hush, N. S. *Prog. Inorg. Chem.* **1967**, *8*, 391. (b) Piepho, S. B.; Krausz, E. R.; Schatz, P. N. *J. Am. Chem. Soc.* **1978**, *100*, 2996. (c) Hartmann, H.; Berger, S.; Winter, R.; Fiedler, J.; Kaim, W. *Inorg. Chem.* **2000**, *39*, 4977. (d) Ernst, S.; Hanel, P.; Jordanov, J.; Kaim, W.; Kasack, V.; Roth, E. *J. Am. Chem. Soc.* **1989**, *111*, 1733. (e) Pratt, R. C.; Stack, T. D. P. *J. Am. Chem. Soc.* **2003**, *125*, 8716. (f) Chang, H.-C.; Mochizuki, K.; Kitagawa, S. *Inorg. Chem.* **2002**, *41*, 4444. (g) Pierpont, C. G. *Coord. Chem. Rev.* **2001**, *219*, 415. (h) Kaim, W.; Schwederski, B. *Pure Appl. Chem.* **2004**, *76*, 351. (i) Ray, K.; Petrenko, T.; Wieghardt, K.; Neese, F. *Dalton Trans.* **2007**, 1552.

(7) (a) Ghumaan, S.; Sarkar, B.; Maji, S.; Puranik, V. G.; Fiedler, J.; Urbanos, F. A.; Jimenez-Aparicio, R.; Kaim, W.; Lahiri, G. K. *Chem.—Eur. J.* **2008**, *14*, 10816. (b) Ye, S.; Sarkar, B.; Duboc, C.; Fiedler, J.; Kaim, W. *Inorg. Chem.* **2005**, *44*, 2843. (c) Kaim, W.; Sarkar, B. *Coord. Chem. Rev.* **2007**, *251*, 584. (d) Ghumaan, S.; Sarkar, B.; Patra, S.; van Slageren, J.; Fiedler, J.; Kaim, W.; Lahiri, G. K. *Inorg. Chem.* **2005**, *44*, 3210. (e) Hendrickson, D. N.; Pierpont, C. G. *Top. Curr. Chem.* **2004**, *234*, 63. (f) Dei, A.; Gatteschi, D.; Pardi, L. *Inorg. Chem.* **1990**, *29*, 1442. (g) Haga, M.; Dodsworth, E. S.; Lever, A. B. P. *Inorg. Chem.* **1986**, *25*, 447.

(8) (a) Lin, C.-Y.; McGlashen, M. L.; Hu, S.; Shim, Y. K.; Smith, K. M.; Spiro, T. G. *Inorg. Chim. Acta* **1996**, *252*, 179. (b) Krejcik, M.; Danek, M.; Hartl, F. *J. Electroanal. Chem. Interfacial Electrochem.* **1991**, *317*, 179.

(9) Sheldrick, G. M. *SHELX-97* (including SHELXS and SHELXL); University of Göttingen: Göttingen, Germany, 1997.

Table 1. Crystallographic Data of $1 \cdot C_7H_8$ and $2 \cdot C_7H_8$

	$1 \cdot C_7H_8$	$2 \cdot C_7H_8$
formula	$C_{61}H_{44}N_4O_{10}Re_2$	$C_{57}H_{42}N_4O_{10}Re_2$
M_r	1365.40	1315.35
cryst syst	triclinic	orthorhombic
space group	$P\bar{1}$	*Pnma*
a (Å)	13.4838(2)	13.2905(2)
b (Å)	13.8023(2)	24.1141(4)
c (Å)	16.2869(3)	15.0699(3)
α (deg)	96.2148(11)	90
β (deg)	111.0004(9)	90
γ (deg)	108.1030(9)	90
V (Å^3)	2606.03(7)	4829.73(14)
Z	2	4
T (K)	150(2)	150(2)
λ (Å)	0.71073	0.71073
D_{calc} (g cm^{-3})	1.740	1.809
μ (mm^{-1})	4.707	5.076
$F(000)$	1336	2568
goodness-of-fit	1.055	1.036
$R_1{}^a/wR_2{}^b$ [$I > 2\sigma(I)$]	0.0357/0.0913	0.0285/0.0715
$R_1{}^a/wR_2{}^b$ (all data)	0.0473/0.0969	0.0443/0.0777
largest residuals (e Å^{-3})	2.098/−1.972	1.602/−1.067

$^a R_1 = \sum||F_o| - |F_c||/\sum|F_o|$. $^b wR_2 = \{\sum[w(F_o^2 - F_c^2)^2]/\sum[w(F_o^2)^2]\}^{1/2}$.

in Table 1; selected bond distances and angles for the two structures are provided in the Supporting Information, Table S1.

Computational Section. The singlet ground-state geometries of complexes **1** and **2** were optimized in the gas phase using the B3LYP[10] functional and the LANL2DZ[11] for the Re core potentials and basis set in the Gaussian 03 program package.[12] The initial geometry was obtained from the crystal structures for **1** and **2**. The 6-31G* basis set[13] was used for all other atoms. Selected parameters of the optimized geometries of **1** and **2** are listed in the Supporting Information, Table S2. Dihedral angles between the aryl groups are also listed in the Supporting Information, Table S3.

The singly reduced geometries of **1** and **2** were calculated using the unrestricted B3LYP functional (UB3LYP) in the gas phase. Ground-state B3LYP optimized geometries were used for geometry optimization in singly reduced states.

To estimate the theoretical values for vertical excitations from the ground state, computations using the TDDFT in the gas phase, the B3LYP hybrid functional, and the 6-31G* basis set were used in the first step. In the second step, the dielectric solvent effects were modeled in the integral equation formalism[14] for the polarizable continuum model[15] (IEF-PCM) in the DMSO (dielectric $\varepsilon = 46.7$).[12] The lowest 55 singlet excited states were calculated using TDDFT/IEF-PCM. DMSO was chosen as the solvent in TDDFT calculations in order to be consistent with the experiment. The output contained information (Table S4 in the Supporting Information) for the excited-state energies and oscillator strengths (f) and a list of the excitations that give rise to each excited state, the orbitals involved, and the wave function coefficients of the excitations.

Finally, to depict the detail of the frontier molecular orbitals, the stereocontour graphs of some related frontier molecular orbitals of the complexes for the ground states and the singly reduced states were drawn with the GView 3.09 program based on the computational results. For orbital contributions, the molecular orbital compositions were analyzed using the AOMIX program.[16]

Synthesis of 1,4-Bis(5,6-dimethylbenzimidazol-1-ylmethyl)-naphthalene (*p*-NBimM) Ligand (L′). KOH (0.095 g, 1.75 mmol) was slowly added to 20 mL of a THF solution of benzimidazole (0.51 g, 3.45 mmol), with stirring, whereupon a white milky suspension appeared to form. Stirring was continued at room temperature for 4 h. After that, 20 mL of a THF solution of 1,4-bis(bromomethyl)naphthalene (0.53 g, 1.7 mmol) was added dropwise, and the reaction mixture was stirred continuously overnight. The solvent was removed under reduced pressure; the reaction mixture was washed thoroughly with water (15 mL × 3) to remove trace base and extracted with dichloromethane (15 mL × 3). The combined organic layer was again washed with water (20 mL) and dried over Na_2CO_3. The crude product was dissolved in hot acetone, followed by the slow addition of petroleum ether (bp 40−60 °C) and then cooling to room temperature to afford a white microcrystalline solid. Yield: 0.37 g, 24%. ^{1}H NMR (400 MHz, DMSO-d_6, 25 °C, relative to $SiMe_4$): δ 8.25 (dd, 2H, J = 3.3 Hz, H^{11}, H^{14}), 8.17 (s, 2H, H^2), 7.65 (dd, 2H, J = 3.3 Hz, H^{12}, H^{13}), 7.42 (s, 2H, H^4), 7.22 (s, 2H, H^7), 6.89 (s, 2H, H^9, H^{10}), 5.91 (s, 4H, H^8), 2.28 (s, 6H, CH_3, *p*-NBimM), 2.22 (s, 6H, CH_3, *p*-NBimM). Anal. Calcd for $C_{30}H_{28}N_4$: C, 81.05; H, 6.35; N, 12.60. Found: C, 80.77; H, 6.13; N, 12.06%. FAB-MS: m/z 444.57 [M^+].

Synthesis of [{Re(CO)$_3$}$_2$(μ-dhnq)(μ-*p*-NBimM)] (1). A mixture of $Re_2(CO)_{10}$ (221 mg, 0.33 mmol), *p*-NBimM (171 mg, 0.32 mmol), and H_2-dhnq (120 mg, 0.34 mmol) in toluene in a Teflon flask was placed in a steel bomb. The bomb was placed in an oven maintained at 160 °C for 72 h and then cooled to 25 °C. Good quality, dark-green single crystals of **1** were obtained. The crystals were separated by filtration, washed with toluene and hexane, and dried in the air. Yield: 74% (198 mg, 0.15 mmol). ^{1}H NMR (400 MHz, DMSO-d_6, 25 °C, relative to $SiMe_4$): δ 8.61 (s, 2H, H^2, *p*-NBimM), 8.38 (m, 4H, H^a, dhnq), 8.10 (m, 2H, H^{14}, *p*-NBimM), 7.89 (s, 2H, H^4, *p*-NBimM), 7.73 (m, 4H, H^b, dhnq), 7.71 (s, 2H, H^7, *p*-NBimM), 7.70 (m, 2H, H^{13}, *p*-NBimM), 7.23 (m, 5H, toluene), 7.15 (s, 2H, H^9, *p*-NBimM), 5.93 (s, 4H, $H^8(-CH_2-)$, *p*-NBimM), 2.29 (s, 3H, CH_3, toluene), 2.25 (s, 6H, CH_3, *p*-NBimM), 1.36 (s, 6H, CH_3, *p*-NBimM). Anal. Calcd for $C_{54}H_{36}N_4O_{10}Re_2 \cdot (C_7H_8)$: C, 53.66; H, 3.25; N, 4.10. Found: C, 53.37; H, 3.32; N, 4.07%. FAB-MS: m/z 1272.15 [M^+].

Synthesis of [{Re(CO)$_3$}$_2$(μ-dhaq)(μ-*p*-NBimM)] (2). A mixture of $Re_2(CO)_{10}$ (219 mg, 0.34 mmol), *p*-NBimM (170 mg, 0.34 mmol), and H_2-dhaq (118 mg, 0.35 mmol) in toluene in a Teflon flask was placed in a steel bomb. The bomb was placed in an oven maintained at 160 °C for 48 h and then cooled to 25 °C. Good quality, dark-green single crystals of **2** were obtained. The crystals were separated by filtration, washed with toluene and hexane, and dried in the air. Yield: 66% (219 mg, 0.18 mmol).

(10) (a) Becke, A. D. *J. Chem. Phys.* **1993**, *98*, 5648. (b) Lee, C.; Yang, W.; Parr, R. G. *Phys. Rev. B* **1988**, *37*, 785. (c) Vosko, S. H.; Wilk, L.; Nusair, M. *Can. J. Phys.* **1980**, *58*, 1200.
(11) Hay, P. J.; Wadt, W. R. *J. Chem. Phys.* **1985**, *82*, 270.
(12) Frisch, M. J.; Trucks, G. W.; Schlegel, H. B.; Scuseria, G. E.; Robb, M. A.; Cheeseman, J. R.; Montgomery, J. A., Jr.; Vreven, T.; Kudin, K. N.; Burant, J. C.; Millam, J. M.; Iyengar, S. S.; Tomasi, J.; Barone, V.; Mennucci, B.; Cossi, M.; Scalmani, G.; Rega, N.; Petersson, G. A.; Nakatsuji, H.; Hada, M.; Ehara, M.; Toyota, K.; Fukuda, R.; Hasegawa, J.; Ishida, M.; Nakajima, T.; Honda, Y.; Kitao, O.; Nakai, H.; Klene, M.; Li, X.; Knox, J. E.; Hratchian, H. P.; Cross, J. B.; Bakken, V.; Adamo, C.; Jaramillo, J.; Gomperts, R.; Stratmann, R. E.; Yazyev, O.; Austin, A. J.; Cammi, R.; Pomelli, C.; Ochterski, J. W.; Ayala, P. Y.; Morokuma, K.; Voth, G. A.; Salvador, P.; Dannenberg, J. J.; Zakrzewski, V. G.; Dapprich, S.; Daniels, A. D.; Strain, M. C.; Farkas, O.; Malick, D. K.; Rabuck, A. D.; Raghavachari, K.; Foresman, J. B.; Ortiz, J. V.; Cui, Q.; Baboul, A. G.; Clifford, S.; Cioslowski, J.; Stefanov, B. B.; Liu, G.; Liashenko, A.; Piskorz, P.; Komaromi, I.; Martin, R. L.; Fox, D. J.; Keith, T.; Al-Laham, M. A.; Peng, C. Y.; Nanayakkara, A.; Challacombe, M.; Gill, P. M. W.; Johnson, B.; Chen, W.; Wong, M. W.; Gonzalez, C.; Pople, J. A. *Gaussian 03*, revision E.01; Gaussian, Inc.: Wallingford, CT, 2003.
(13) (a) Stratmann, R. E.; Scuseria, G. E.; Frisch, M. J. *J. Chem. Phys.* **1998**, *109*, 8218. (b) Bauernschmitt, R.; Ahlrichs, R. *Chem. Phys. Lett.* **1996**, *256*, 454. (c) Casida, M. E.; Jamorski, C.; Casida, K. C.; Salahub, D. R. *J. Chem. Phys.* **1998**, *108*, 4439.
(14) (a) Mennucci, B.; Tomasi, J. *J. Chem. Phys.* **1997**, *106*, 5151. (b) Tomasi, J.; Mennucci, B.; Cancés, E. *J. Mol. Struct. THEOCHEM* **1999**, *464*, 211.
(15) Tomasi, J.; Menucci, B.; Cammi, R. *Chem. Rev.* **2005**, *105*, 2999.
(16) (a) Gorelsky, S. I. AOMIX. http://www.sg-chem.net (accessed Sep 2010). (b) Gorelsky, S. I.; Lever, A. B. P. *J. Organomet. Chem.* **2001**, *187*, 635.

Scheme 1. Self-Assembly of Metallacycles **1** and **2**

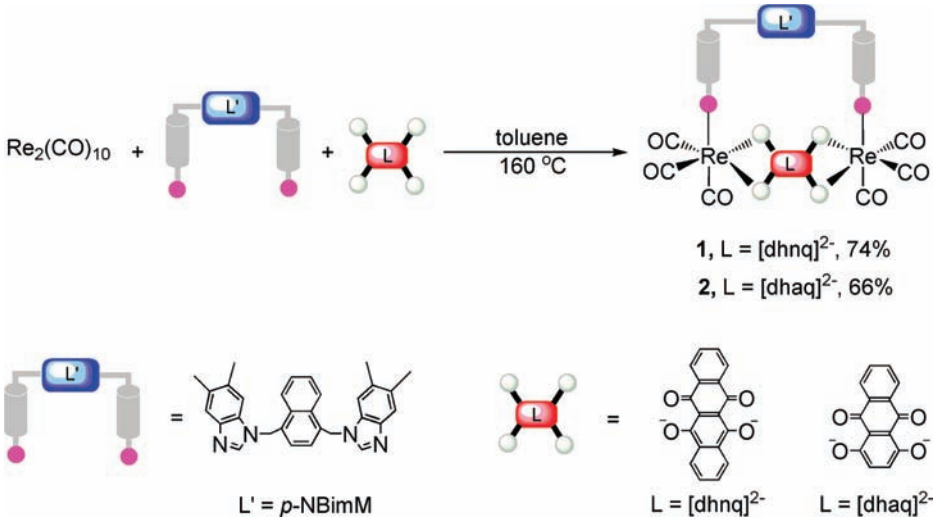

^{1}H NMR (400 MHz, DMSO-d_6, 25 °C, relative to $SiMe_4$): δ 8.65 (s, 2H, H^2, *p*-NBimM), 8.30 (d, 2H, H^b dhaq), 8.17 (m, 2H, H^{14}, *p*-NBimM), 7.82 (s, 2H, H^4, *p*-NBimM), 7.76 (m, 6H, H^a, H^c, dhaq; H^{13}, *p*-NBimM), 7.22 (m, 2H, H^7, *p*-NBimM), 7.18 (m, 5H, toluene), 7.02 (s, 2H, H^9, *p*-NBimM), 6.08−5.96 (s, 4H, $H^8(-CH_2-)$, *p*-NBimM), 2.29 (s, 3H, CH_3, toluene), 2.25 (s, 6H, CH_3, *p*-NBimM), 2.05 (s, 6H, CH_3, *p*-NBimM). Anal. Calcd for $C_{50}H_{34}N_4O_{10}Re_2$: C, 49.09; H, 2.80; N, 4.58. Found: C, 48.97; H, 2.79; N, 4.47%. FAB-MS: *m*/*z* 1224.14 [M^+].

Results and Discussion

Synthesis and Characterization. The synthesis of dirhenium(I) metallacycles [{$Re(CO)_3$}$_2$(μ-L)(μ-L′)] (**1**, L = $dhnq^{2-}$; **2**, L = $dhaq^{2-}$; H_2dhnq = 6,11-dihydroxy-5,12-naphthacenedione; H_2dhaq = 1,4-dihydroxy-9,10-anthraquinone; L′ = 1,4-bis(5,6-dimethylbenzimidazol-1-ylmethyl)-naphthalene, *p*-NBimM) via the orthogonal bonding approach is shown in Scheme 1.[5d,17] The synthetic approach involved the simultaneous introduction of a bis-chelating, quinone-based moiety to interface with two *fac*-$Re(CO)_3$ cores and a ditopic semirigid *N*-donor ligand, *p*-NBimM, to the remaining orthogonal site, leading to the formation of chair-shaped metallacycles in high yields. The products are air- and moisture-stable and are soluble in polar organic solvents. Compared to the free ligands, ^{1}H NMR signals of the quinone moieties were shifted downfield (atom numbering for ^{1}H NMR assignments are in the Supporting Information, Figure S1).[18] Infrared carbonyl stretching frequencies of these complexes exhibit tricarbonyl stretching patterns in the 1880−2050 cm^{-1} range.[5,19] The FAB mass spectra of **1** and **2** showed molecular ion peaks at *m*/*z* 1272.15 and 1224.14, respectively. The structures of complexes **1** and **2** were further confirmed by single-crystal X-ray diffraction analysis.

X-Ray Structural Details and Computed Geometries. ORTEP and perspective diagrams of complexes **1** and **2** are shown in Figures 1 and 2 and in the Supporting Information, Figure S2, along with pertinent crystallographic data, and selected bond distances and angles can be found in Tables 1 and S1 (Supporting Information), respectively. Single-crystal X-ray diffraction analysis revealed that the *p*-NBimM ligand in **1** and **2** adopts a *syn* conformation and serves as a molecular clip to bind the two *fac*-$Re(CO)_3$ cores, which are paired by a dianionic doubly chelating quinone-based ligand ($dhnq^{2-}$ for **1** and $dhaq^{2-}$ for **2**), using the adjacent phenolate and quinone oxygens, resulting in an octahedrally coordinated C_3NO_2 environment around the rhenium centers. Dirhenium(I) metallacycles **1** and **2** have Re···Re distances of 8.608 and 8.622 Å, respectively. Of note, the dihedral angle between the two benzimidazole groups of the *p*-NBimM ligand in **1** is smaller than that in **2**. As a result, **1** has a "closed" chairlike structure, while **2** is a widely "opened up" metallacycle (Figure S3 and Table S3 in the Supporting Information). In addition, the shortest nonbonding distance between naphthalene-C of the *p*-NBimM ligand and the dhnq/dhaq plane is 4.01 Å for **1** and 4.60 Å for **2** (Figure S3 in the Supporting Information).

A comparison of selected bond lengths and bond angles with optimized geometries is presented in Table S2 of the Supporting Information. The bond lengths and angles obtained by the DFT calculations for the two complexes in the ground state were very similar (difference in bond length is less than 0.06 Å) to the experimentally determined structure. In the series, the experimental Re−N and Re−O bond lengths were 2.19 and 2.09 Å for **1**, respectively. The results of a DFT study indicate that the bond distances for Re−N and Re−O in compound **1** are 2.25 and 2.13 Å, respectively. The DFT bond length for **2** is very similar to that of **1**, as shown in Table S2.

Molecular Orbitals. On the basis of the DFT/B3LYP/6-311G* theoretical framework, the ground-state electronic structure was calculated to determine the energies and additional single-point energy calculations for compositions of the molecular orbitals (MOs) using the optimized geometries of **1** and **2**. The assignment of the type of each MO was made on the basis of its composition and by

(17) (a) Sathiyendiran, M.; Wu, J.-Y.; Velayudham, M.; Lee, G.-H.; Peng, S.-M.; Lu, K.-L. *Chem. Commun.* **2009**, 3795. (b) Liao, R.-T.; Yang, W.-C.; Thanasekaran, P.; Tsai, C.-C.; Sathiyendiran, M.; Liu, Y.-H.; Rajendran, T.; Lin, H.-M.; Tseng, T.-W.; Lu, K.-L. *Chem. Commun.* **2008**, 3175. (c) Sathiyendiran, M.; Liao, R.-T.; Thanasekaran, P.; Luo, T.-T.; Venkataramanan, N. S.; Lee, G.-H.; Peng, S.-M.; Lu, K.-L. *Inorg. Chem.* **2006**, *45*, 10052.
(18) Su, C. Y.; Cai, Y. P.; Chen, C. L.; Smith, M. D.; Kaim, W.; zur Loye, H. C. *J. Am. Chem. Soc.* **2003**, *125*, 8595.
(19) Blanco-Rodríguez, A. M.; Towrie, M.; Collin, J.-P.; Zális, S.; Vlček, A., Jr. *Dalton Trans.* **2009**, 3941.

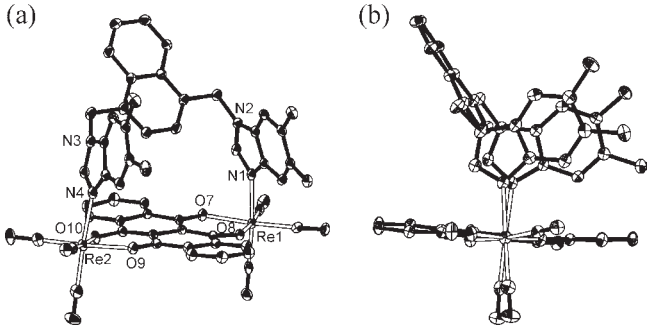

Figure 1. (a) Slightly off front view and (b) side view of the molecular structure of **1** (ORTEP plot with 30% thermal ellipsoids). Hydrogen atoms are omitted for clarity.

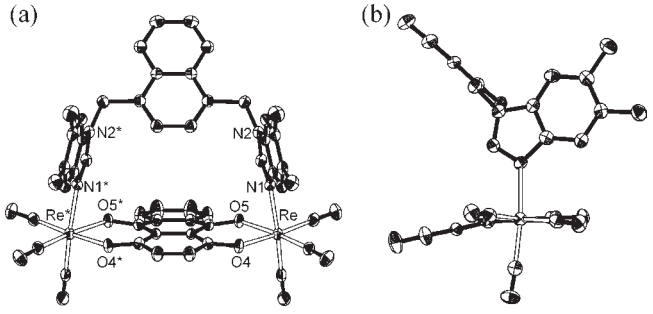

Figure 2. (a) Front view and (b) side view of the molecular structure of **2** (ORTEP plot with 50% thermal ellipsoids). Hydrogen atoms are omitted for clarity.

visual inspection of its three-dimensional representation. Selected frontier molecular orbitals and their relative energies were computed and are shown in Figure 3. Complexes **1** and **2** have HOMO−LUMO gaps of 2.54 and 2.36 eV, respectively. Although the trend for the calculated LUMO energies of **1** and **2** is inconsistent with the observed reduction potential, the first singlet−singlet transition of **2** is found to be more red-shifted than that of **1**, which is in line with the trend observed in the electronic absorption spectra (vide infra). Quinones are noninnocent and thus provide high-lying, filled π orbitals.[20] Thus, the HOMO of **1** contained 76% $dhnq^{2-}$ ligand. The HOMO of **2** is quite similar to that of **1**, with 73% of its population as the dhaq ligand. The LUMO of complexes **1** and **2** contained $\geq$90% π^* orbitals of the quinone. The calculated molecular orbital isosurface plots in the SOMOs of radical anions, $\mathbf{1}^{\bullet-}$ and $\mathbf{2}^{\bullet-}$, essentially LUMOs of **1** and **2**, were spread over the π^* orbital of the quinone ring (Figure S4, in the Supporting Information).

Photophysical Properties. The UV−vis absorption spectra were recorded in DMSO solutions at 298 K (Figure 4, and Table 2). TDDFT calculations with a solvation model (Table S4 in the Supporting Information) indicated that the main transitions of complexes **1** and **2** in the 550−640 nm range are probably excitation of the quinonoid ligand with some contributions from metal−ligand charge transfer (MLCT) transitions.[21] The experimentally determined absorption bands at 387 nm in **1** and 413 nm in **2**, respectively, can be attributed to intense MLCT+LLCT transitions [394 nm, HOMO−6 → LUMO (66%); 422 nm, HOMO−5 → LUMO (66%)] for **1** and **2**, (Figure S5 and Table S4 in the Supporting Information). The peak positions are red-shifted in the theoretical spectra; nevertheless, the trends observed for the relative transition energies between **1** and **2** are consistent. For example, the transition energy for the first excited state of **1** is higher (2.26 eV) than that of **2** (2.11 eV). A similar trend is observed in the experimental absorption band (605 nm in **1** and 640 nm in **2**).

The free *p*-NBimM ligand exhibited fluorescence at 333 and 390(sh) nm with a lifetime of 5.8 ns, whereas the quinones emitted in the 537−565 nm regions with a lifetime of >2 ns (Figure S7 and Table S5 in the Supporting Information) in deoxygenated THF. Upon excitation at the MLCT position in a THF solution at 298 K under nitrogen, complexes **1** and **2** displayed emissions at 467, 534, 570(sh), and 644 nm and 475, 540, and 554(sh) nm, respectively (Figure S8 in the Supporting Information).[5d,22] The emissions observed at ~470 and 535 nm are tentatively assigned to the LLCT transition and intraligand $^1\pi-\pi^*$ transition of quinone ligands, respectively, whereas the weak emission of **1** observed at 644 nm can be attributed to a Re → *p*-NBimM metal-to-ligand charge transfer transition (Table S5 in the Supporting Information).[23] These assignments were further confirmed by recording the emission spectra of **1** and **2** in THF at 77 K (Figure S9 in the Supporting Information). Low temperature emission spectra of **1** and **2** clearly show a well-defined Re → *p*-NBimM metal-to-ligand charge transfer transition at 615 nm, which can be attributed to a Re−N coordinated MLCT transition.[24] To confirm the presence of multiple excited states, the excitation spectra of **1** and **2** were recorded, and the uncorrected excitation spectra are shown in Figure S8 in the Supporting Information. The excitation spectra of **1** showed that the emission at 467 nm is due to a LLCT transition, and the emission at 534 nm is assigned to the intraligand $^1\pi-\pi^*$ transition of the quinone ligand. Similar behavior was observed in the case of the excitation spectra of **2**. The emission decays had lifetimes (τ) of 12.1 and 14.3 ns for **1** and **2**, respectively (Figure S10 in the Supporting Information), which can be attributed to the fluorescence lifetime of an admixture of singlet $\pi-\pi^*$ of *p*-NBimM and a quinone moiety.

Electrochemistry. The disodium salts of quinones and metallacycles **1** and **2** were investigated by cyclic voltammetry (DMSO, 298 K, $[Bu_4N][ClO_4]$ (0.1 M) as the supporting electrolyte, vs SCE.

The cyclic voltammogram (CV) of the dianionic quinones reveals up to two possible electron additions (Table 3 and Figure S11 in the Supporting Information), which are assigned to the $[L]^{2-} \rightarrow [L]^{3\bullet-}$ and $[L]^{3\bullet-} \rightarrow [L]^{4-}$ reductions (Scheme 2).[1f,7g] The clip benzimidazolate ligand contributes no redox properties within the solvent window, as evidenced by a CV investigation. Because the complexes

(20) Pierpont, C. G.; Francesconi, L. C.; Hendrickson, D. N. *Inorg. Chem.* **1978**, *17*, 3470.
(21) (a) Lynch, M. W.; Hendrickson, D. N.; Fitzgerald, B. J.; Pierpont, C. G. *J. Am. Chem. Soc.* **1984**, *106*, 2041. (b) Buchanan, R. M.; Pierpont, C. G. *J. Am. Chem. Soc.* **1980**, *102*, 4951.
(22) (a) DeArmond, M. K.; Carlin, C. M. *Coord. Chem. Rev.* **1981**, *36*, 325. (b) Song, L.-Q.; Feng, J.; Wang, X.-S.; Yu, J.-H.; Hou, Y.-J.; Xie, P.-H.; Zhang, B.-W.; Xiang, J.-F.; Ai, X.-C.; Zhang, J.-P. *Inorg. Chem.* **2003**, *42*, 3393. (c) Tyson, D. S.; Luman, C. R.; Zhou, X.; Castellano, F. N. *Inorg. Chem.* **2001**, *40*, 4063.
(23) Glazer, E. C.; Magde, D.; Tor, Y. *J. Am. Chem. Soc.* **2005**, *127*, 4190.
(24) Thanasekaran, P.; Liao, R. T.; Liu, Y. H.; Rajendran, T.; Rajagopal, S.; Lu, K. L. *Coord. Chem. Rev.* **2005**, *249*, 1085.

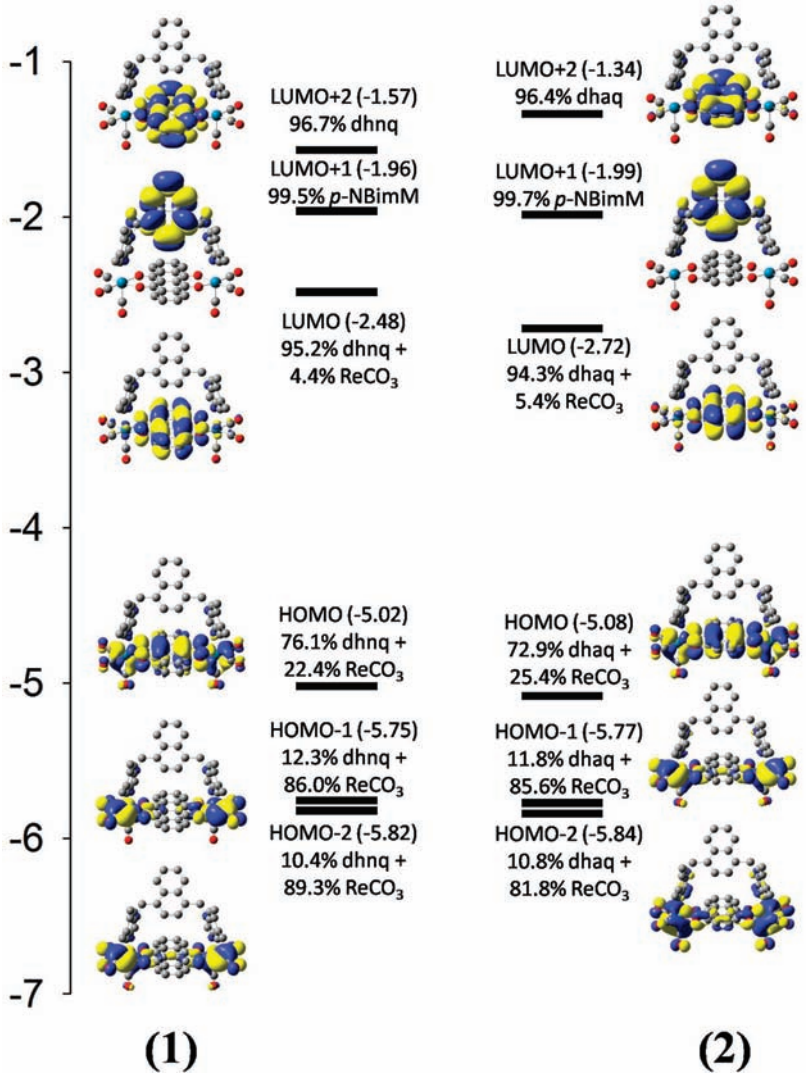

Figure 3. Frontier molecular orbitals for the most relevant terms of compounds **1** (left) and **2** (right, isodensity value = 0.02) calculated using B3LYP functionals and LANL2DZ ECP, with the IEF-PCM solvent model. MO energies are in electrovolts. AOMIX breakdowns of relevant MOs into constituent components are in parentheses.

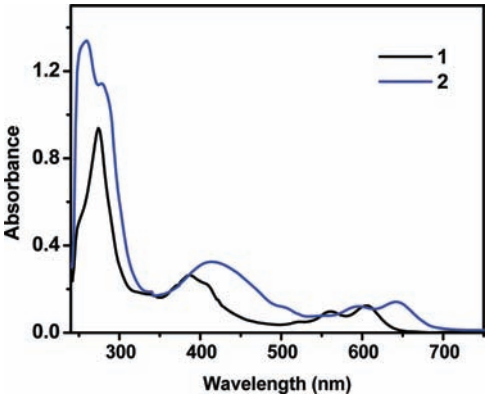

Figure 4. Electronic absorption spectra of complexes **1** (black) and **2** (blue) in DMSO solution (10^{-4} M) at 298 K.

contain one quinone moiety, two successive one-electron ligand-based reduction waves would be expected. Figure 5 shows CV data for **1** and **2**. As the potential was scanned from zero to the negative region, **1** accepts an electron to become a radical anion at a half-wave potential of −0.70 V then gains a second electron to likely become a dianion at a half-wave potential of −1.22 V (Figure 5a). The half-wave potentials for the two consecutive reductions of **2** were −0.88 and −1.36 V vs SCE, respectively (Figure 5b). The current ratio is good, and the plot of currents vs $\nu^{1/2}$ is used to identify that the reaction is diffusion controlled. The first and second quinone reductions for the **1** and **2** assemblies were cathodically shifted compared to the redox potentials of the free dianionic quinone analogs.[25] The differences are inconsistent with the expectation of electrostatic stabilization of the negatively charged, reduced forms of the ligands by the coordinated rhenium cations.[26] This shifting is more evident in **1** compared to that of **2**. Moreover, the Re(I/0) reduction was not observed within the solvent window (+0.7 to −2.8 V). The large differences in potentials between the two successive reduction processes point

(25) Peover, M. E. *J. Chem. Soc.* **1962**, 4540.

(26) (a) Sun, S.-S.; Lees, A. J. *J. Am. Chem. Soc.* **2000**, *122*, 8956. (b) Gosztola, D.; Niemczyk, M. P.; Svec, W.; Lukas, A. S.; Wasielewski, M. R. *J. Phys. Chem. A* **2000**, *104*, 6545. (c) O'Reilly, J. E.; Elving, P. J. *J. Am. Chem. Soc.* **1972**, *94*, 7941. (d) Knödler, A.; Wanner, M.; Fiedler, J.; Kaim, W. *J. Chem. Soc., Dalton Trans.* **2002**, 3079.

Table 2. Absorption Maxima[a] from UV−vis−NIR Data in Various Oxidation States From OTTLE Spectroelectrochemistry[b]

	n		
compound	0	−1	−2
Na_2dhnq	267 (1513), 383 (1188), 410 (922), 456 (211), 485 (338), 517 (303), 563 (60.7)	287 (1917), 383 (1188), 535 (715), 729 (72.3), 944 (49.1), 1079 (66.7), 1255 (72.3)	295 (1672), 377 (533), 488 (sh) (416), 526 (724), 716 (83.6), 798 (77.5)
Na_2dhaq	278 (909), 331 (sh) (272), 471 (715.8)	308 (525), 389 (586.5), 496 (2170), 681 (181.7), 764 (227), 854 (184)	336 (sh) (322.3), 477 (2071.4), 563 (346.6)
1	275 (7456), 387 (1458.6), 518 (sh) (395.8), 559 (763.7), 605 (1011.4)	292 (7395.6), 392 (898.7), 436 (sh) (787), 524 (sh) (638.6), 582 (1905.8), 804 (247), 1012 (191.5), 1170 (433), 1397 (601.5)	305 (6918.7), 529 (1765.8), 768 (620), 853 (620)
2	275 (4519.4), 413 (1317.6), 587 (479.1), 640 (621.8)	274 (6418.2), 393 (sh) (835.3), 537 (1263.5), 866 (461.4)	280 (6244.4), 472 (1248.3), 609 (589)

[a] Absorption maxima λ_{max} in nm, molar absorption coefficient $\varepsilon \times 10^{-3}$ (in parentheses) in M^{-1} cm^{-1}. [b] From measurement in 0.1 M Bu_4NClO_4/DMSO.

Table 3. Electrochemical Data from Cyclic Voltammetry[a,b]

	Na_2dhnq	Na_2dhaq	*p*-NBimM	**1**	**2**
$E_{1/2}$ (red1)	−0.55 (70)	−0.71 (30)	−	−0.70 (70)	−0.88 (60)
$E_{1/2}$ (red2)	−1.11 (60)	−1.18 (50)	−	−1.22 (45)	−1.36 (60)

[a] Potential in V vs SCE are listed, with peak potential differences in parentheses, scan rate 100 mV s^{-1}. [b] In 0.1 mM Bu_4NClO_4/DMSO.

to a large thermodynamic stability for the intermediate radical anions, $\mathbf{1}^{\bullet-}$ and $\mathbf{2}^{\bullet-}$. It is much easier to reduce the $dhnq^{2-}$ moiety in **1** than reduce the $dhaq^{2-}$ moiety in **2** (Figure 5).

UV−vis−NIR Spectro-Electrochemistry. The redox reactions of **1** and **2** were investigated via UV−vis−NIR SEC measurements using an optically transparent thin-layer electrochemical (OTTLE) technique[8] to establish the likely sites of electron transfer: the accessible reductions for the states with $n = 0, -1$, and -2 (Figures 6 and 7 and Table 2). With knowledge of the redox potentials of **1**, **2**, Na_2dhnq, and Na_2dhaq, it is now possible to generate certain reduced states of these compounds electrochemically and to identify their characteristic signatures in the corresponding UV−vis−NIR spectra. Figures 6 and 7 illustrate the development of the absorption bands as a function of time of **1** and **2**, respectively.

Among the two singly reduced radical complexes, the symmetrically bridged quinone complex **1** shows a strong absorption in the NIR region, which is absent in the neutral and doubly reduced states. The behavior of **1** in the singly and doubly reduced states is analogous to that of Na_2dhnq quinone.

The electronic spectrum of **1** changed substantially upon reduction to $\mathbf{1}^{\bullet-}$, particularly in the lower-energy region. A reduction from the $\mathbf{1} \rightarrow \mathbf{1}^{\bullet-}$ state (Figure 6a) caused the MLCT absorption band at $\lambda_{max} = 387$ nm (black curve) to progressively red-shift with a constant drop in intensity, and the ILCT band ($\lambda_{max} = 559$ and 605 nm) merged with a new, higher intensity band at $\lambda_{max} = 582$ nm (Figure 6a, blue curve). This is probably a consequence of the sequential addition of electrons to the empty π^* orbitals of the ligand. After reduction, the energy of these orbitals is increased, and the MLCT transition is shifted to a higher energy.[5d,6c] This is accompanied by the appearance of several new absorption bands at 804, 1012, 1170, and 1397 nm, which are characteristics of the radical anion form of Na_2dhnq (Figure S13, in the Supporting Information). The π^* MO of the quinone ring is considerably stabilized through the 4-fold coordination of the two

Scheme 2. Redox Chart (**1**, L = dhnq; **2**, L = dhaq; L′ = *p*-NBimM)

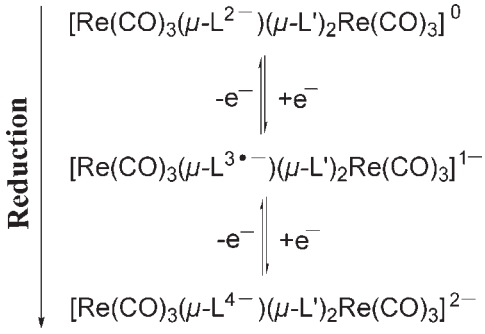

σ-electrophilic *fac*-$Re(CO)_3$ moieties, and thus all of the peaks are red-shifted in $\mathbf{1}^{\bullet-}$ compared to $[dhnq]^{3\bullet-}$.[5d,6c] Interestingly, $\mathbf{1}^{\bullet-}$ exhibited an intense NIR band at 1397 nm ($\varepsilon = 601.5$ M^{-1} cm^{-1}), which were absent in both the neutral and dianionic forms. The intense lowest-energy absorption was an internal π (SOMO) → π^* ILCT transition of the quinone radical anion. The presence of two isosbestic points at $\lambda = 433$ and 630 nm indicates a clean conversion from $\mathbf{1} \rightarrow \mathbf{1}^{\bullet-}$ without the formation of intermediates or byproducts.

Upon successive reduction, i.e., $\mathbf{1} \rightarrow \mathbf{1}^{\bullet-} \rightarrow \mathbf{1}^{2-}$, the d$\pi$ Re(I) → π^* ligand MLCT transition completely disappeared, and an ILCT band in the visible region was blue-shifted to 529 nm from 582 nm (Figure 6b). Two new peaks are generated at 767 and 853 nm in $\mathbf{1}^{2-}$ and are probably due to the ILCT of the quinone, which is also observed in $[dhnq]^{4-}$ (Figure S13, right in the Supporting Information). The large blue-shift from the NIR to the visible range upon double reduction is due to the subsequent addition of an electron and an increase in the π^* MO energy of the quinone ring.[5d] Furthermore, the electrochemical measurements indicate that conversion between the $\mathbf{1} \rightarrow \mathbf{1}^{\bullet-}$ and the $\mathbf{1}^{\bullet-} \rightarrow \mathbf{1}^{2-}$ states is nearly 94% and 99% reversible, respectively. The number of electrons transferred during this reaction was further established using absorbance-applied potential titrations (Figure S12 in the Supporting Information).

In contrast, the one electron reduction of **2** to the $\mathbf{2}^{\bullet-}$ state did not dramatically alter the electronic spectrum (Figure 7). The ILCT transitions are blue-shifted from 587 and 640 to 537 nm and increase in intensity. Similar to $\mathbf{1} \rightarrow \mathbf{1}^{\bullet-}$, the MLCT peak is progressively red-shifted with a constant drop in intensity. One broad signal at 866 nm upon the reduction of $\mathbf{2} \rightarrow \mathbf{2}^{\bullet-}$ occurred. This behavior

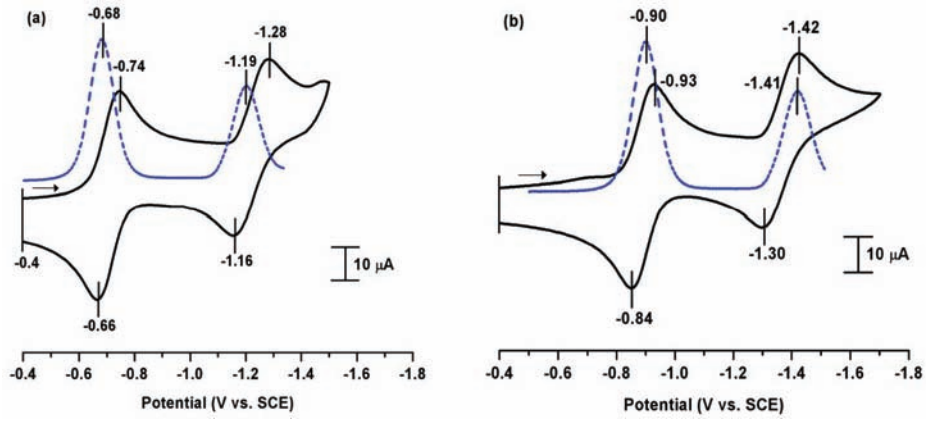

Figure 5. Cyclic voltammograms (black, solid line) and differential pulse voltammograms (blue, broken line) (showing reduction potential only) of **1** (left) and **2** (right) in DMSO (1 mM) in 0.1 M $[Bu_4N][ClO_4]$ with a scan rate of 100 mV/s vs Ag/AgCl.

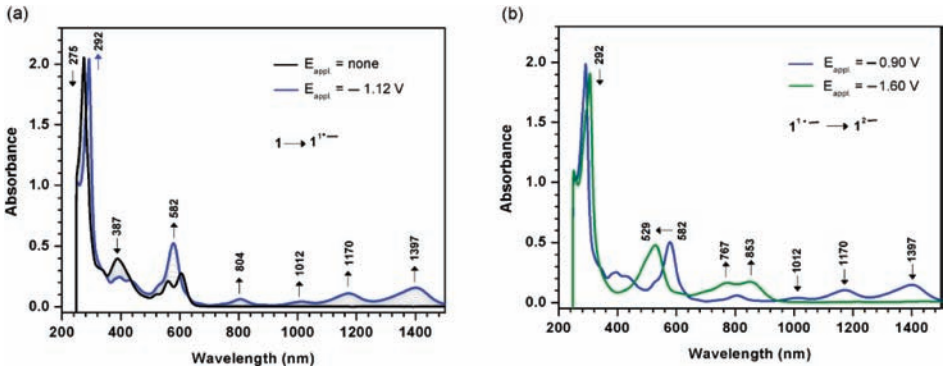

Figure 6. UV−vis−NIR spectra of (a) **1** (black, left) and $\mathbf{1}^{\bullet-}$ (blue, left) and (b) $\mathbf{1}^{\bullet-}$ (blue, right) and $\mathbf{1}^{2-}$ (olive, right) under increasing cathodic potential in 0.1 M TBAP in DMSO at 25 °C. Concentration: $[\mathbf{1}] = 2.77 \times 10^{-4}$ M.

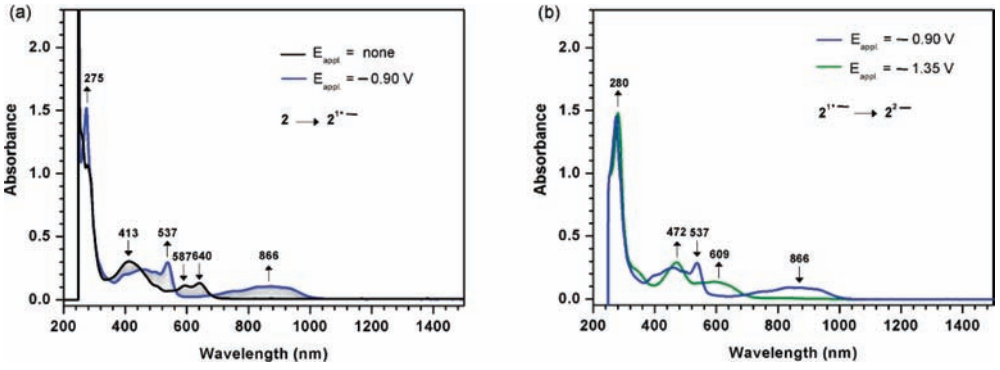

Figure 7. UV−vis−NIR spectra of (a) **2** (black, left) and $\mathbf{2}^{\bullet-}$ (blue, left) and (b) $\mathbf{2}^{\bullet-}$ (blue, right) and $\mathbf{2}^{2-}$ (olive, right) under increasing cathodic potential in 0.1 M TBAP in DMSO at 25 °C. Concentration: $[\mathbf{2}] = 2.37 \times 10^{-4}$ M.

is characteristic of the $[dhaq]^{3\bullet-}$ (Figure S14, in the Supporting Information). A further one electron reduction of $\mathbf{2}^{\bullet-}$ caused an ILCT band in the visible region to be further blue-shifted to 472 nm from 537 nm and the ILCT band of the quinone was shifted to 609 nm from 866 nm, as was also observed in the successive reduction of **1**. Electrochemical measurements indicate that the conversion between the $\mathbf{2} \rightarrow \mathbf{2}^{\bullet-}$ and the $\mathbf{2}^{\bullet-} \rightarrow \mathbf{2}^{2-}$ states is nearly 97% and 95% reversible, respectively.

The difference in spectral behavior in the singly reduced states of quinones and also in the metallacycles is probably due to the annealed benzene ring in **1** and $dhnq^{2-}$ because of its symmetric π-electron system, which is perturbed to a lesser degree compared to the asymmetric quinonoid-bridged **2** and the free quinone, $dhaq^{2-}$. Thus, combinations arising from this special situation are summarized in Scheme 2 (L = $dhnq^{2-}$ in **1** and $dhaq^{2-}$ in **2**). Furthermore, the spin distribution in terms of the valence-bond description, which represents the contribution of all the possible resonance structures of the radical anion of quinone, is shown in Scheme 3.

Electron Spin Resonance. The identities of singly reduced species, generated via the use of cobaltocene (Cp_2Co) as a reducing agent in DMSO at room temperature, were further characterized in the form of glassy frozen solutions by X-band ESR spectroscopy. The rhombic ESR signal

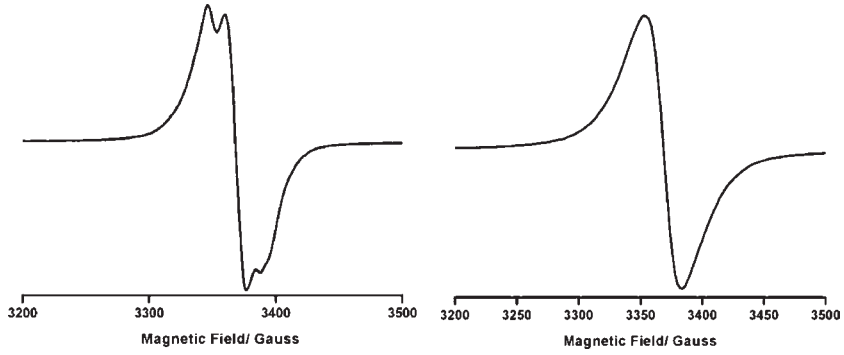

Figure 8. EPR spectra [X-band, DMSO, at 77 K] (concentration: 10^{-2} M; microwave frequency 9.6127, microwave power 40 mW, modulation amplitude 7.75 G, modulation frequency 100 kHz) of $\mathbf{1}^{\bullet-}$ ($g_1 = 2.012$, $g_2 = 2.006$, $g_3 = 1.9875$, left) and $\mathbf{2}^{\bullet-}$ ($g = 2.0008$, right).

Scheme 3. Spin Distribution in Terms of Valence-Bond Description Representing the Contribution of All of the Resonance Structures

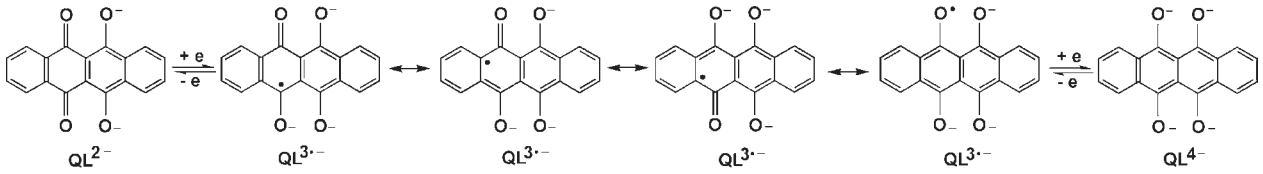

in $\mathbf{1}^{\bullet-}$ was observed ($g_1 = 2.012$, $g_2 = 2.006$, $g_3 = 1.9875$, $g_{avg} = 2.0018$, $\Delta = g_1 - g_3 = 0.024$ at 77 K; Figure 8, left).[27] In contrast to $\mathbf{1}^{\bullet-}$, a free radical signature in the EPR spectrum was observed for $\mathbf{2}^{\bullet-}$; i.e., the g value of $\mathbf{2}^{\bullet-}$ ($g_{iso} = 2.0008$) was consistent with the absence of any contribution by metal orbitals (the same as the free-electron value) to the SOMO of $\mathbf{2}^{\bullet-}$ (Figure 8, right).[28] The electron spin density showed a typical pattern for a semiquinone-like structure on each ring (Figure S15 in the Supporting Information).[29] The spin density analysis is consistent with the observed Δg value, in that the SOMO for $\mathbf{1}^{\bullet-}$ and $\mathbf{2}^{\bullet-}$ was distributed mainly on the quinonoid ligand with a 5% contribution from the dπ−Re orbital in $\mathbf{1}^{\bullet-}$ and even less in $\mathbf{2}^{\bullet-}$.

Judging from the ESR spectra, the alternatives to the redox redistributed form, $[(CO)_3Re^0(\mu\text{-}L^{\bullet-})(\mu\text{-}L')Re^0(CO)_3]^{\bullet-}$, are less compatible with the absence of Re−quinone orbital mixing and thus superexchange interactions in the singly reduced metallacycles. The absence of a metal-based spin in the singly reduced states further rules out the possibility of any redox redistribution.

Summary and Conclusions

In summary, two new chair-shaped dirhenium(I) metallacycles, based on quinonoid ligands, were designed and prepared in high yields. Electrochemical assessments using CV and UV−vis−NIR SEC of these new complexes revealed that they were quinone ligand-centered; two well-separated, single-electron, reversibly accessible 0, −1, and −2 redox states, while the benzimidazolate ligand appears to be redox innocent within the solvent window. The combined investigations reveal that the singly reduced metallacycles are best described as highly stable, noncommunication, localized, quinonoid-centered radical complexes, $[(CO)_3Re^I(\mu\text{-}L^{3\bullet-})(\mu\text{-}L')Re^I(CO)_3]^{\bullet-}$, with less compatible metal-based spin characteristics, via redox redistribution.

Acknowledgment. We thank Academia Sinica and the National Science Council of Taiwan for financial support.

Supporting Information Available: X-ray crystallographic files (CIF) of **1** and **2**, atom numbering for ^{1}H NMR assignments, photophysical data of **1** and **2**, electrochemical data of ligands, absorbance-applied potential titration plots, geometry optimized Cartesian coordinates (Tables S6−S9). This material is available free of charge via the Internet at http://pubs.acs.org.

(27) (a) Berger, S.; Klein, A.; Kaim, W. *Inorg. Chem.* **1998**, *37*, 5664. (b) Klein, A.; Vogler, C.; Kaim, W. *Organometallics* **1996**, *15*, 236.

(28) (a) Ho, T.-I.; Creber, K. A. M.; Wan, J. K. S. *J. Am. Chem. Soc.* **1981**, *103*, 6524. (b) Creber, K. A. M.; Wan, J. K. S. *J. Am. Chem. Soc.* **1981**, *103*, 2101.

(29) (a) Mattar, S. M. *J. Phys. Chem. B* **2004**, *108*, 9449. (b) Mattar, S. M.; Stephens, A. D. *Chem. Phys. Lett.* **1999**, *306*, 249. (c) Morley, J. O. *J. Phys. Chem.* **1995**, *99*, 5956.